

Subdominant d -wave interaction in superconducting $\text{CaKFe}_4\text{As}_4$?

D. Jost,^{1,2} J.-R. Scholz,^{1,2} U. Zweck,^{1,2} W. R. Meier,^{3,4}
A. E. Böhmer,^{4,*} P. C. Canfield,^{4,3} N. Lazarević,⁵ and R. Hackl¹

¹Walther Meissner Institut, Bayerische Akademie der Wissenschaften, 85748 Garching, Germany

²Fakultät für Physik E23, Technische Universität München, 85748 Garching, Germany

³Department of Physics and Astronomy, Iowa State University, Ames, Iowa 50011, USA

⁴Division of Materials Science and Engineering, Ames Laboratory, Ames, Iowa 50011, USA

⁵Center for Solid State Physics and New Materials, Institute of Physics Belgrade,
University of Belgrade, Pregrevica 118, 11080 Belgrade, Serbia

(Dated: May 31, 2018)

We report inelastic light scattering results on the stoichiometric and fully ordered superconductor $\text{CaKFe}_4\text{As}_4$ as a function of temperature and light polarization. In the energy range between 10 and 315 cm^{-1} (1.24 and 39.1 meV) we observe the particle-hole continuum above and below the superconducting transition temperature T_c and 7 of the 8 Raman active phonons. The main focus is placed on the analysis of the electronic excitations. Below T_c all three symmetries projected with in-plane polarizations display a redistribution of spectral weight characteristic for superconductivity. The energies of the pair-breaking peaks in A_{1g} and B_{2g} symmetry are in approximate agreement with the results from photoemission studies. In B_{1g} symmetry the difference between normal and superconducting state is most pronounced, and the feature is shifted downwards with respect to those in A_{1g} and B_{2g} symmetry. The maximum peaking at 134 cm^{-1} (16.6 meV) has a substructure on the high-energy side. We interpret the peak at 134 cm^{-1} in terms of a collective Bardasis-Schrieffer (BS) mode and the substructure as a remainder of the pair-breaking feature on the electron bands. There is a very weak peak at 50 cm^{-1} (6.2 meV) which is tentatively assigned to another BS mode.

PACS numbers: 74.70.Xa, 74.20.Mn, 74.25.nd

I. INTRODUCTION

$\text{CaKFe}_4\text{As}_4$ is among the few iron-based compounds which are superconducting at high transition temperature T_c at stoichiometry¹ since the Ca and K atoms form alternating intact layers as shown in Fig. 1. The high degree of order allows one to get as close to the intrinsic properties of the material class as possible since the effects of disorder are expected to be negligible or at least significantly smaller than in solid solutions such as $\text{Ba}_{1-x}\text{K}_x\text{Fe}_2\text{As}_2$ or $\text{Ba}(\text{Fe}_{1-x}\text{Co}_x)_2\text{As}_2$. For instance the residual resistivity ratio (RRR) reaches 15 and is much higher than for $\text{Ba}(\text{Fe}_{1-x}\text{Co}_x)_2\text{As}_2$ and comparable or better than for $\text{Ba}_{1-x}\text{K}_x\text{Fe}_2\text{As}_2$ ². Other transport and the thermodynamic properties² highlight the similarities to optimally or overdoped $\text{Ba}_{1-x}\text{K}_x\text{Fe}_2\text{As}_2$.

These similarities include the electronic structure, in particular the Fermi surfaces [Fig. 1 (c)] and the superconducting energy gaps³. The gaps were found to be rather isotropic on the individual bands having values of $2\Delta_\alpha = 21\text{ meV}$, $2\Delta_\beta = 24\text{ meV}$, $2\Delta_\gamma = 16\text{ meV}$ and $2\Delta_\delta = 24\text{ meV}$ on the three hole bands (α , β , γ) and the electron band (δ), respectively. The good nesting observed between the β and δ bands was considered to support s -wave interband pairing³⁻⁵ as proposed earlier for the iron-based materials in general⁶.

Since there is also nesting among the electron bands one can expect a competing pairing interaction with d -wave symmetry as a subleading instability⁷. Indications thereof were found recently in Raman scattering experiments on $\text{Ba}_{1-x}\text{K}_x\text{Fe}_2\text{As}_2$ ⁸⁻¹⁰. The subleading channel

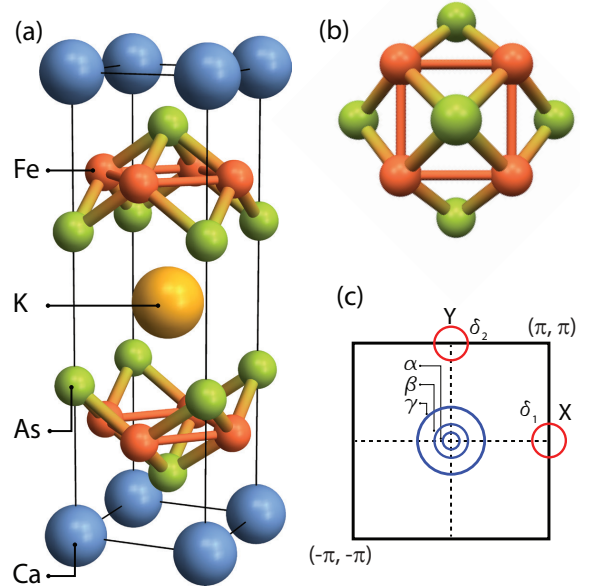


Figure 1. Structure and Fermi surface of $\text{CaKFe}_4\text{As}_4$. (a) Tetragonal unit cell with the Ca, K, Fe, and As atoms shown in blue, gold, red, and respectively, green¹. (b) Quasi 2D Fe_2As_2 layer with the full orange line depicting the 1 Fe unit cell. (c) Brillouin zone of the 1 Fe cell. The three hole bands labeled α , β , and γ (blue) encircle the Γ point. The electron bands δ_1 and δ_2 (red) are centered at the X and Y point, respectively [adopted from Mou *et al.*³].

manifests itself as a narrow line below the gap edge given that the gap is clean as, e.g., in $\text{Ba}_{1-x}\text{K}_x\text{Fe}_2\text{As}_2$ ¹¹⁻¹³.

The bound state has its origin in a phase fluctuation of the condensate of Cooper pairs. The experimental identification of this excitation as a Bardasis-Schrieffer (BS) exciton rests on the shape of the line, its temperature dependence and the spectral weight transfer from the pair-breaking feature to the in-gap mode as described in detail in Refs. 9 and 10.

Given its nearly clean gap and the high crystal quality, $\text{CaKFe}_4\text{As}_4$ is an excellent candidate for scrutinizing the superconducting properties of hole doped 122 systems. We aim at answering the question as to whether or not subleading channels can also be observed in systems other than $\text{Ba}_{1-x}\text{K}_x\text{Fe}_2\text{As}_2$ and can be identified as generic.

II. EXPERIMENT

Calibrated Raman scattering equipment was used for the experiments. The sample was attached to the cold finger of a He-flow cryostat. For excitation a diode-pumped solid state laser emitting at 575 nm (Coherent GENESIS MX-SLM 577-500) was used. The polarization of the incoming light was adjusted in a way that the light inside the sample had the proper polarization state. The absorbed power (inside the sample) was set at typically $P_a = 2$ mW independent of polarization. By setting the polarizations of the incident and scattered photons the four symmetries A_{1g} , A_{2g} , B_{1g} , and B_{2g} of the D_{4h} space group can be accessed. For the symmetry assignment we use the 1 Fe unit cell [see Fig. 1 (b) and (c)] since the density of states at the Fermi energy E_F is nearly entirely derived from Fe orbitals. The related projections in the first Brillouin zone (BZ) are visualized in Fig. A1 of Appendix A. In this work the focus is placed on low energies, where A_{2g} is negligibly small. The polarization combinations RR , xy , and $x'y'$ almost exclusively project the A_{1g} , B_{2g} , and B_{1g} symmetries as desired. Here x and y are horizontal and vertical, respectively, in the laboratory system. Note that the out-of-phase vibration of the Fe atoms appears in B_{2g} symmetry in the 1 Fe unit cell rather than in B_{1g} symmetry of the crystallographic unit cell hosting two Fe atoms per Fe_2As_2 plane. For more details see section B. The spectra are represented as response functions $R\chi''(T, \Omega)$ which are obtained by dividing the measured cross section by the thermal Bose factor $\{1 + n(\Omega, T)\} = \{1 + [\exp(\hbar\omega/k_B T) - 1]^{-1}\}$. R is an experimental constant.

The $\text{CaKFe}_4\text{As}_4$ single crystals were grown from the FeAs flux and characterized thoroughly as described by Meier and coworkers^{2,14}. The T_c value of 35.21 ± 0.10 K we found here is in the range 35.0 ± 0.2 K determined by Meier *et al.* (see Fig. C in Appendix A3). The crystal structure of $\text{CaKFe}_4\text{As}_4$ is very similar to that of AFe_2As_2 systems [cf. Fig. 1 (a)] and belongs to the tetragonal D_{4h} space group. Since $\text{CaKFe}_4\text{As}_4$ has alternating Ca and K planes between the Fe_2As_2 layers the point group is simple-tetragonal ($P4/mmm$)¹ rather than the body-centered tetragonal ($I4/mmm$) as

BaFe_2As_2 [15].

III. RESULTS

Fig. 2 shows the normal (red) and superconducting (blue) Raman spectra of $\text{CaKFe}_4\text{As}_4$ at the three polarization configurations (a) RR , (b) xy , and (c) $x'y'$. The sample is rotated by 45° with respect to the orientation in Figs. 1 and A1 in order to suppress any c -axis projection in the B_{1g} spectra (xy in the laboratory system). Superimposed on the particle-hole continua we observe six and four phonons in RR and $x'y'$ polarization, respectively¹⁶ which will be discussed in Appendix B. As intended there are no phonons in xy configuration, and the spectrum in the normal state is completely smooth to within the experimental error. The structure-less shape indicates that there is no polarization leakage and, more importantly, that there is no defect-induced scattering from phonons highlighting the high crystal quality. We focus now exclusively on the electronic continua.

To this end we also plot the difference spectra,

$$\Delta R\chi''(\Omega) = R\chi''(T = 11 \text{ K}, \Omega) - R\chi''(T = 43 \text{ K}), \quad (1)$$

(orange in Fig. 2) along with the raw data of each polarization configuration. In the difference spectra $\Delta R\chi''(\Omega)$ temperature-independent structures such as (most of) the phonons and the presumably weak and temperature-independent luminescence contributions are eliminated. In this way the changes induced by superconductivity are highlighted.

All spectra show the typical changes upon entering the superconducting state: (i) The opening of the gap induces a suppression of the intensity below a cross-over energy of $\Omega_0 = 125$, 115, and 130 cm^{-1} for A_{1g} , B_{1g} , and B_{2g} symmetry, respectively. In this range $\Delta R\chi''(\Omega)$ (orange) is negative. (ii) The intensity piles up above Ω_0 due to a coherent superposition of pair-breaking and Bogoliubov quasiparticle excitations across the gap 2Δ . The amplitude of the redistribution is small in A_{1g} and B_{2g} symmetry [Fig. 2 (a) and (c) and Figs. A4 and A6] but pronounced in B_{1g} symmetry. [Fig. 2 (b) and Fig. A5]. In the A_{1g} response [Fig. 2 (a)] the signal at $\Omega \rightarrow 0$ is enhanced because of surface layers of accumulating residual gas molecules at low temperature (see Fig. A4) and the insufficient suppression of the elastically scattered light in the case of parallel light polarizations (RR here).

The first striking observation is the nearly symmetry-independent cross-over energy Ω_0 where the normal (red) and superconducting (blue) spectra intersect each other or where $\Delta R\chi''(\Omega)$ changes sign. Yet, the intensity for $\Omega < \Omega_0$ does not vanish entirely as expected for a clean gap but is only reduced. No additional structures are observed in the A_{1g} and B_{2g} spectra while a weak hump appears at approximately 50 cm^{-1} [see Fig. 2 (b) and arrows in Fig. 3 (b) to (f)] in B_{1g} symmetry. It appears also at elevated temperatures as shown in Fig. A5 and is therefore considered a robust feature.

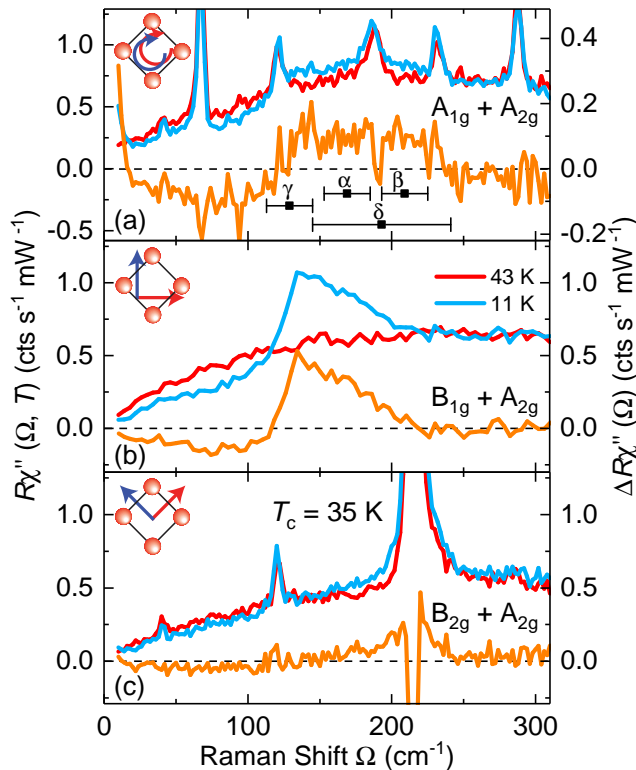


Figure 2. Raman response in $\text{CaKFe}_4\text{As}_4$ at symmetries and polarizations as indicated. Shown are raw data for $T \ll T_c$ (blue), $T > T_c$ (red) and difference spectra (orange). Phonon modes are present in the A_{1g} and B_{2g} spectra. (a) The pair-breaking maximum extends from $\Omega_0^{(A_{1g})} = 120 \pm 2 \text{ cm}^{-1}$ to $\Omega_m \approx 230 \text{ cm}^{-1}$. The gap energies $2\Delta_i$ for the four bands i observed by ARPES³ are reproduced as horizontal bars. (b) The B_{1g} pair-breaking peak is well defined and sets on at $\Omega_0^{(B_{1g})} = 116 \pm 5 \text{ cm}^{-1}$. The dashed line at low energies indicates the expected spectral dependence for a clean gap. (c) The weak B_{2g} pair-breaking peak is located slightly above $2\Delta_\beta$. The intersection of the normal and superconducting spectra is close to $\Omega_0^{(B_{2g})} = 130 \pm 5 \text{ cm}^{-1}$.

Second, whereas the normal and the superconducting spectra merge at similar energies close to $\Omega_m = 230 \text{ cm}^{-1}$ in all symmetries the distribution of spectral weight in the range $\Omega_0 < \Omega < \Omega_m$ varies substantially. In none of the symmetries the pair-breaking features display the typical shape. The pair-breaking maximum in B_{2g} symmetry is found at approximately 215 cm^{-1} right underneath the Fe phonon. The negative intensity at 215 cm^{-1} shows that the phonon is renormalized below T_c , and an influence of this renormalization on the electronic features cannot be excluded. However, the gap below 130 cm^{-1} indicates the presence of an intensity redistribution below T_c . In A_{1g} symmetry a wide plateau is observed between Ω_0 and Ω_m . Finally in B_{1g} symmetry, a pronounced peak is found at 135 cm^{-1} above which the intensity decays. Upon studying various temperatures a secondary maximum at about 165 cm^{-1} can be resolved

as shown in Fig. A5 in the .

For the discussion below we additionally plot in Fig. 2 (a) the gap energies $2\Delta_i$ as horizontal bars according to a recent photoemission study³, where i is the band index [c.f. Fig. 1 (c)]. The width of the bars corresponds to the error bars of order $\pm 10\%$ indicated there.

IV. DISCUSSION

The main purpose of this section is a balanced discussion of the possible interpretations of the electronic Raman spectra presented in section III. Can the spectra be interpreted exclusively in terms of pair-breaking or are collective modes, similarly as in $\text{Ba}_{1-x}\text{K}_x\text{Fe}_2\text{As}_2$, necessary for a more consistent explanation?

A. Gap energies

Using yellow excitation we find a strong redistribution of spectral weight in B_{1g} symmetry similarly as in a simultaneous Raman study using red photons¹⁷ (Note that B_{1g} and B_{2g} are interchanged in these studies.) With yellow photons the redistribution can be observed in all three symmetry channels. As already noticed earlier this difference in the experimental results may be traced back to orbital dependent resonance effects¹⁰.

The highest pair-breaking energy in our study is observed in B_{2g} symmetry implying a maximal gap energy of $2\Delta_{\max} \approx 215 \text{ cm}^{-1}$. This energy corresponds to $\Delta_{\max} = 13.3 \text{ meV}$ slightly higher than the largest gaps derived for the β and δ bands, $\Delta_{\beta,\delta} = 12 \text{ meV}$ using angle-resolved photoemission spectroscopy (ARPES)³. 215 cm^{-1} coincides with the edge of the A_{1g} pair-breaking feature [see Fig. 2], and we conclude that the ARPES data slightly underestimate the gap energies found by Raman scattering as already observed for $\text{Ba}_{1-x}\text{K}_x\text{Fe}_2\text{As}_2$ [8 and 9]. Similarly, the lowest gap energy of $\Delta_\gamma = 8 \text{ meV}$ is below 9.3 meV expected from the lower edge in the A_{1g} spectra. There are no structures in the A_{1g} and B_{2g} spectra which one could associate with the gap energy on the α band, $\Delta_\alpha = 10.5 \text{ meV}$, obtained from ARPES. On this basis we conclude that the maximal gap energies derived from the A_{1g} and B_{2g} Raman spectra are in the same range of approximately $9 k_B T_c$ as in $\text{Ba}_{1-x}\text{K}_x\text{Fe}_2\text{As}_2$ close to optimal doping⁹.

The question arises whether ARPES and Raman results are compatible with the selection rules. As shown in Fig. A1 all bands should be visible in A_{1g} symmetry with comparable weight upon neglecting resonance effects. In fact, all energies are represented in the spectra shown in Fig. 2 (a). Even if a Leggett mode contributes to the A_{1g} spectra, as suggested recently¹⁸, this conclusion survives since the Leggett modes are expected close to the maximal gap energies in the Fe-based systems. The B_{2g} spectra are less easily to be reconciled with this

scenario since the gaps on the hole bands should be projected with a similar spectral weight as that of the electron band. Yet we find only a contribution from the largest gap. Although the overall intensity is very weak here the absence of contributions from the γ band cannot be explained by the variation of the peak height with $|\Delta|^2$ [19] or by applying the symmetry selection rules. Either a phenomenological treatment as for $\text{Ba}_{1-x}\text{K}_x\text{Fe}_2\text{As}_2$ [9] or a detailed resonance study needs to be performed which, however, is beyond the scope of this work.

Given that the single particle gap energies are by and large reproduced in the A_{1g} and B_{2g} spectra it is important to understand the B_{1g} spectra. As shown in Fig. 2 (c) the energies appearing there are well below those of the A_{1g} and B_{2g} spectra. This is particularly surprising as the δ bands are expected to be projected fully (and not marginally) in B_{1g} symmetry (see Fig. A1) as opposed to all hole bands. Thus, the argument that the strongest peak in the B_{1g} spectra results from the γ band can be discarded.

B. B_{1g} Response

There is only one alternative scenario which reconciles the results observed in the three Raman active symmetries and the ARPES results: The B_{1g} spectra do not directly reflect gap energies but rather are shifted downward by final state interaction as discussed for $\text{Ba}_{1-x}\text{K}_x\text{Fe}_2\text{As}_2$ in earlier work⁸⁻¹⁰. The similarity can be observed directly by comparing the data in Fig. 3. The difference spectra as a function of temperature indicate that the B_{1g} peak has a robust shoulder on the high-energy side. The overall shape is surprisingly similar to the spectra of $\text{Ba}_{0.65}\text{K}_{0.35}\text{Fe}_2\text{As}_2$.

Following this reasoning we identify the maximum of the B_{1g} spectra at 135 cm^{-1} with a collective mode pulled off the maximal gap energy on the δ band due to a $d_{x^2-y^2}$ wave subleading interaction among the two electron bands predicted theoretically¹³ and observed in $\text{Ba}_{1-x}\text{K}_x\text{Fe}_2\text{As}_2$. The hump at approximately 165 cm^{-1} is then the remaining intensity of the pair-breaking peak on the δ band after switching on the final state interaction which induces a transfer of intensity from the pair-breaking peak into the bound state^{9,12,13}. Only in this way the missing intensity in the range of $2\Delta_\delta$ can be explained consistently.

It is tempting to explain the faint peak close to 50 cm^{-1} ($2k_B T_c$) in terms of a second BS mode in a similar fashion as in $\text{Ba}_{1-x}\text{K}_x\text{Fe}_2\text{As}_2$ ¹⁰. This would mean that the subdominant coupling is already very strong, and $\text{CaKFe}_4\text{As}_4$ is on the brink of a d -wave instability. The very weak intensity of the peak argues in this direction since the BS mode is expected to vanish when d -wave pairing wins. Yet, the vanishingly small intensity is also the Achilles heel of the argumentation, and a robust statement is possible only on the basis of a microscopic model, which includes the derivation of the eigenvectors

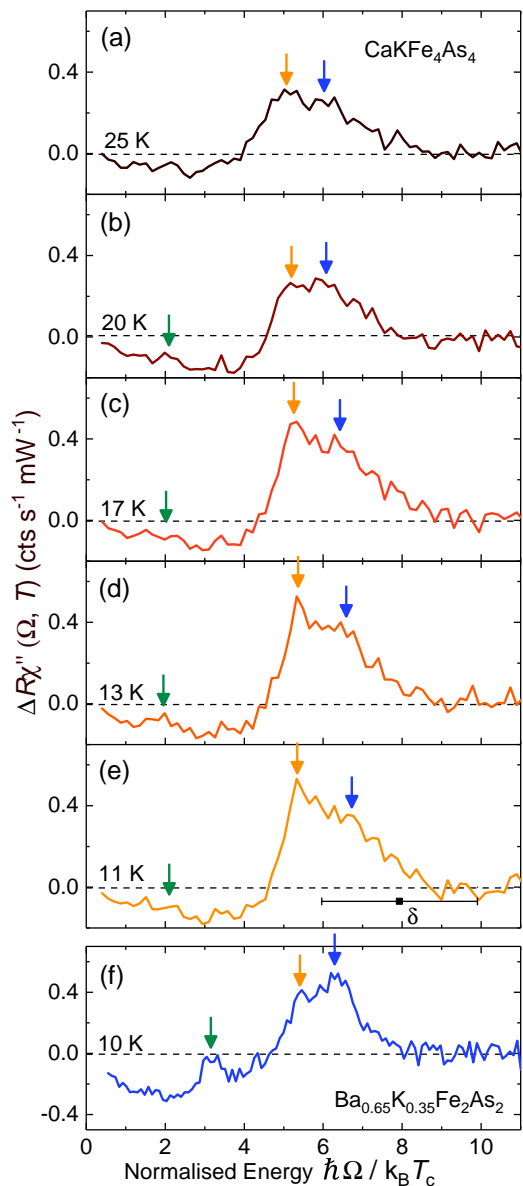


Figure 3. Difference spectra of the B_{1g} Raman response for temperatures as indicated. The main peak exhibits a double structure (orange and blue arrows). A second hump is visible from 25 K down to 13 K (green arrow, see also the raw data in Fig. 2). (f) Difference spectrum of $\text{Ba}_{0.65}\text{K}_{0.35}\text{Fe}_2\text{As}_2$. From¹⁰. The arrows show two Bardasis-Schrieffer modes at 3.1 (green arrow) and $5.2 k_B T_c$ (orange arrow). The remainder of the pair breaking peak is located at $6.2 k_B T_c$ (blue arrow) since the high-energy part is drained into the BS modes.

of the subdominant pairing channels, as proposed for $\text{Ba}_{1-x}\text{K}_x\text{Fe}_2\text{As}_2$ ¹⁰. Such an expensive theoretical treatment is beyond the scope of this experimental study.

V. CONCLUSION

We investigated the recently discovered superconductor $\text{CaKFe}_4\text{As}_4$ with inelastic light scattering as a function of photon polarisation and temperature. Using yellow light (575 nm) superconducting features were found in A_{1g} , B_{1g} and B_{2g} symmetry.

A weak but well-defined pair-breaking feature is found at 215 cm^{-1} (corresponding to $\Delta = 13.3\text{ meV}$) in B_{2g} symmetry which is slightly above the largest gaps observed by ARPES for the β and the δ bands³ and close to the energy Ω_m where the normal and the superconducting spectra merge in all symmetry projections. This feature is also present in the A_{1g} spectra. In addition to the high-energy feature the A_{1g} intensity displays a plateau-like shape down to $\Omega_0^{(A_{1g})} = 125\text{ cm}^{-1}$. Given the small discrepancies between the gap energies derived from the ARPES data and the Raman spectra one can conclude that the A_{1g} spectra reflect the entire range of gap energies of $\text{CaKFe}_4\text{As}_4$ even though the individual gap energies cannot be resolved.

In B_{1g} symmetry, the superconducting feature is centered at lower energy than in the two other symmetries. We interpret the sharp maximum at 135 cm^{-1} as a collective Bardasis-Schrieffer mode pulled off the maximal gap on the δ band similarly as in the sister compound $\text{Ba}_{0.65}\text{K}_{0.35}\text{Fe}_2\text{As}_2$. The shoulder at approximately 165 cm^{-1} is a remainder of the pair-breaking peak losing most of its intensity to the collective mode^{9,13}. Whether or not the weak structure at 50 cm^{-1} is another BS mode with even stronger coupling cannot be decided with certainty because of the fading intensity. If this interpretation could be supported further $\text{CaKFe}_4\text{As}_4$ would be closer to a d -wave instability than $\text{Ba}_{1-x}\text{K}_x\text{Fe}_2\text{As}_2$. The smaller T_c of $\text{CaKFe}_4\text{As}_4$ argues in this direction since a strong d pairing channel frustrates the s -wave ground state and reduces T_c . Even without dwelling on the peak at 50 cm^{-1} we may conclude that $\text{CaKFe}_4\text{As}_4$ is a true sibling of $\text{Ba}_{1-x}\text{K}_x\text{Fe}_2\text{As}_2$ ¹⁰ thus demonstrating that pairing fingerprints can be observed preferably in materials with clean gaps.

ACKNOWLEDGEMENTS

We acknowledge valuable discussions with G. Blumberg. The work was supported by the Friedrich-Ebert-Stiftung, the Transregional Collaborative Research Center TRR 80, and the Serbian Ministry of Education, Science and Technological Development under Project III45018. We acknowledge support by the DAAD through the bilateral project between Serbia and Germany (grant numbers 56267076 and 57142964). Work at Ames Laboratory was supported by the U.S. Department of Energy, Office of Basic Energy Sciences, Division of Materials Sciences and Engineering under Contract No. DE-AC02-07CH11358. W.R.M. was supported by the

Gordon and Betty Moore Foundations EPiQS Initiative through Grant No. GBMF4411.

Appendix A: Raman Selection Rules

Using different combinations of light polarizations different parts of the Brillouin zone can be projected independently for particle-hole excitations²⁰. The weighting factors for the three Raman-active in-plane symmetries are shown in Fig. A1. Here the linear vertices are displayed which are derived entirely on the basis of symmetry arguments. In A_{1g} symmetry we use the second order vertex $\gamma_{A_{1g}}^{(2)} \propto \cos(k_x) \cos(k_y)$ which reflects the band structure better than the first order vertex because of the curvature of the hole and the electron bands^{9,21}. (The zero-order vertex is a constant and entirely screened.)

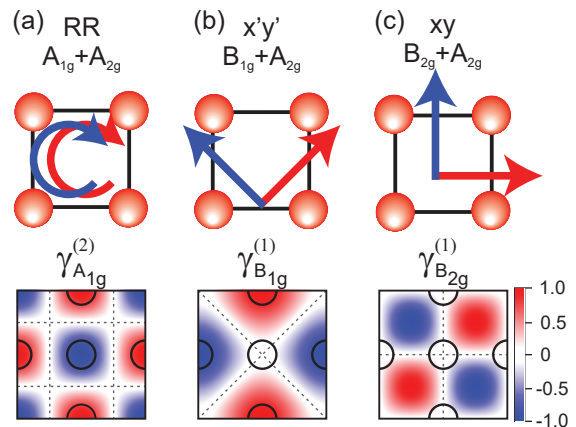


Figure A1. Raman form factors. The first row shows the polarizations w.r.t. the Fe sublattice. The second row displays the momentum dependences of the Raman vertices¹⁹. The A_{1g} vertex displayed here corresponds to $\gamma_{A_{1g}}^{(2)}$ which was found to be the most appropriate vertex for the FeAs systems^{9,21} because of the opposite curvature of the electron and hole bands.

For the experiments the samples were mounted on the cold finger in a way that the crystallographic axes match the laboratory system (xy). Because of the large angle of incidence, the incoming photons having polarization x' or R have the same finite projection on the c -axis. Consequently, E_g phonons, obeying xz and yz selection rules, are expected to appear in both RR and $x'y'$ scattering configurations, whereas they are absent in xy configuration.

Appendix B: Phonons

For the phonons it is more appropriate to use the crystallographic 2Fe unit cell of $\text{CaKFe}_4\text{As}_4$ having $P4/mmm$ symmetry as shown in Fig. 1. The orientation of the crystal in the experiment is displayed as an inset

Table I. Phonon energies of CaKFe₄As₄ at 43 K.

pol	unit	$E_g^{(1)}$	$A_{1g}^{(As1)}$	$E_g^{(2)}$	$A_{1g}^{(As2)}$	$B_{1g}^{(Fe)}$	$E_g^{(3)}$	$A_{1g}^{(Fe)}$
RR	cm^{-1}	42	66	120	188		232	288
	meV	5.21	8.18	14.9	23.3	26.7	28.8	35.7
$x'y'$	cm^{-1}	42		120		215	232	

in Fig. A2. The energies of all phonon lines observed are collected in Table I.

The strongest line that appears at 215 cm^{-1} in $x'y'$ polarization is the out-of-phase c -axis Fe vibration having the proper B_{1g} symmetry in the crystallographic (2 Fe) unit cell.

The in-phase c -axis vibrations of the As atoms appear at 66 and 188 cm^{-1} in the RR spectra. The line at 288 cm^{-1} corresponds to the in-phase c -axis vibrations of the Fe atoms. Three modes appear simultaneously with approximately the same intensity in RR and $x'y'$ polarization both of which having the same finite projection of about 30% on the c -axis of the incoming photons inside the crystal and are tentatively identified as three of the four E_g modes expected to be Raman-active in the $P4/mmm$ structure of CaKFe₄As₄. They are projected

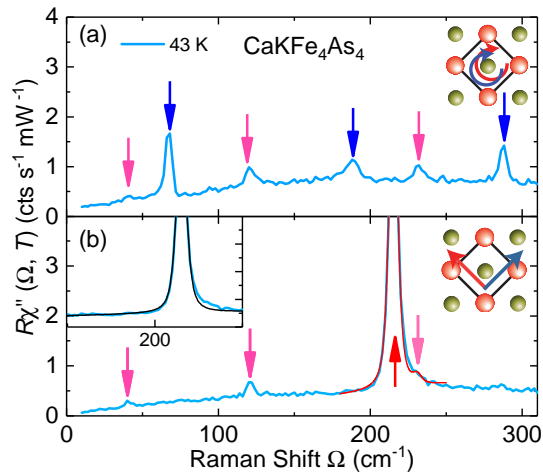


Figure A2. Raman-active phonons in CaKFe₄As₄ at 43 K. The six and four lines in (a) RR and, respectively, (b) $x'y'$ polarization are marked by blue, red, and magenta arrows for A_{1g} , B_{1g} , and E_g symmetry, respectively. The orientation of the crystal with respect to the laboratory frame along with the polarization symbols is shown pictorially with Fe and As displayed in red and olive, respectively. Due to the large angle of incidence of 66° both polarization configurations have a finite projection on the c -axis of the crystal. Thus the E_g phonons are seen with approximately the same intensity in RR and $x'y'$. The E_g mode at 232 cm^{-1} is hidden underneath the B_{1g} mode. The asymmetry of the B_{1g} line can be explained entirely by a superposition of two lines as shown in (b). The inset in (b) shows the data and a symmetric Lorentz line.

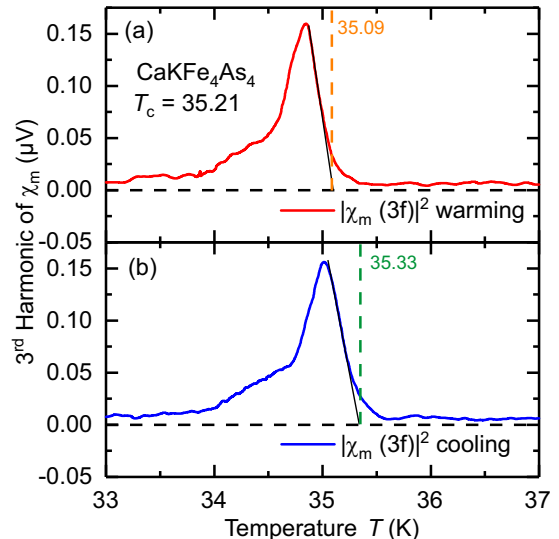


Figure A3. Nonlinear susceptibility of CaKFe₄As₄. The two panels show the signal of the (a) heating and (b) cooling run. Since the sample lags slightly behind the sensor the indicated temperature is slightly higher and lower, respectively, between the curves. We derive $T_c = 33.2 \text{ K}$ and $\Delta T_c = 0.3 \text{ K}$.

in zx and zy configuration thus have only approximately 10% of the full intensity. The mode at 232 cm^{-1} cannot be observed independently in the $x'y'$ spectra since it is too close to the B_{1g} mode. We show an approximate decomposition in Fig. A2 (b). All E_g phonons are shear modes with the Fe and As atoms moving parallel to the FeAs planes with different eigenvectors. In total one expects four E_g modes¹⁶. The missing fourth mode is either too weak to be observable or outside the range we studied.

Appendix C: Sample characterization

The transition temperature T_c of CaKFe₄As₄ sample used for the experiments was determined via the temperature dependence of the nonlinear magnetic susceptibility $\chi_m^{(3)}(T)$ which is very sensitive for sample inhomogeneities²². Fig. A3 displays the results of the measurements on the samples used here for a cooling and a heating run.

As shown by Shatz and coworkers²³ the $\chi_m^{(3)}(T)$ curves displays a nearly linear onset right below T_c given that there is no dc field, the amplitude of the exciting ac field is small (typically $\mu_0 H_0 < 10^{-3} B_{c1}$), and the superconducting transition is sharp ($\Delta T_c \rightarrow 0$). Below T_c $\chi_m^{(3)}(T)$ peaks at an amplitude-dependent temperature and decays again. The extrapolation to zero of the linear part between the peak and T_c can be identified with the midpoint of the transition and T_c can be identified with the midpoint of the transition obtained from the linear susceptibility. If ΔT_c is not negligible $\chi_m^{(3)}(T)$ has a foot above

the extrapolated T_c value. The width of the foot indicates ΔT_c .

Upon measuring $\chi_m^{(3)}(T)$ during cooling and heating with typical rates of ± 1 K per min a small hysteresis of $0.1 \dots 0.2$ K results. We use the average of the two individual T_c values, $T_c = 33.21$ K, as the sample's transition temperature. $\Delta T_c = 0.3$ K can be derived from the foot of $\chi_m^{(3)}(T)$ above T_c . The transition temperature is identical to that of Ref.². We cannot identify any secondary phases.

Appendix D: Raw Data

The left panels of Figs. A4, A5, and A6 show the raw data (after division by the Bose factor) above T_c and at various temperatures below T_c for $\text{CaKFe}_4\text{As}_4$. The difference spectra according to Eq. (1) are shown in the right column.

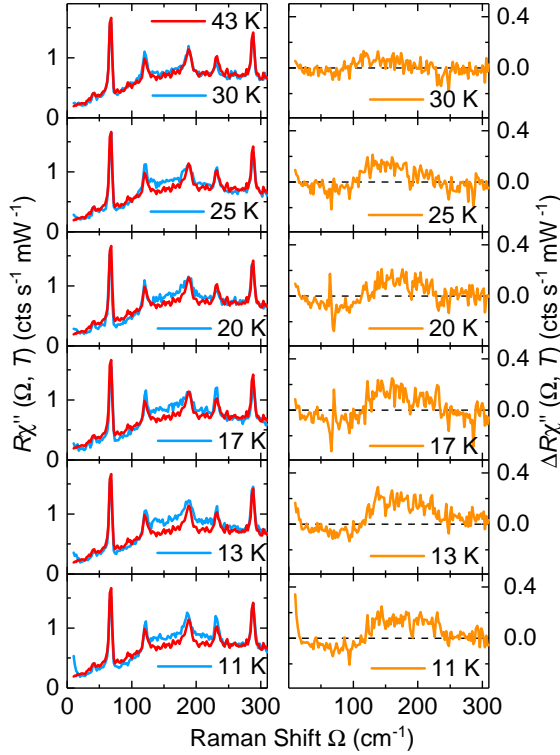


Figure A4. A_{1g} response of $\text{CaKFe}_4\text{As}_4$ for 43 K and temperatures below T_c as indicated. The raw response is shown on the left, the difference spectra are on the right.

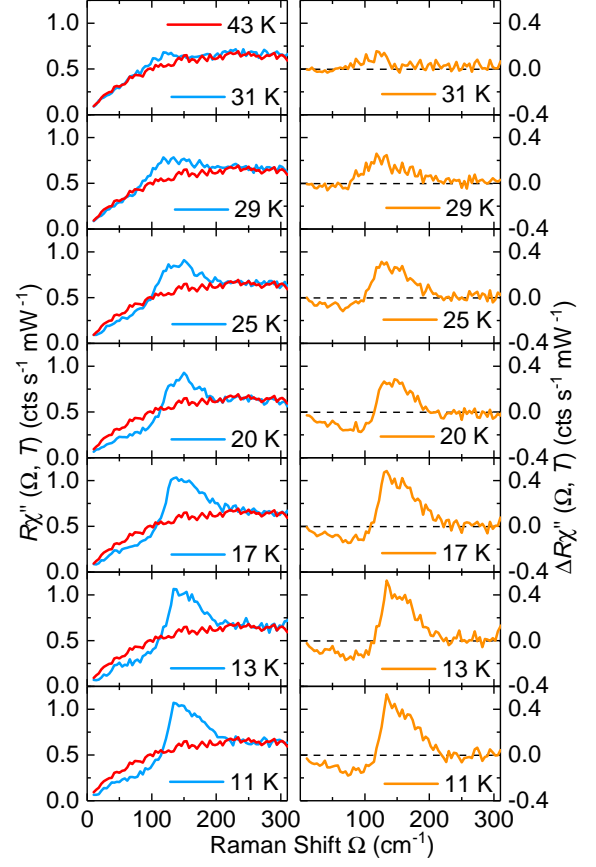


Figure A5. B_{1g} response of $\text{CaKFe}_4\text{As}_4$ for 43 K and temperatures below T_c as indicated. The raw response is shown on the left, the difference spectra are on the right. Close to 50 cm^{-1} there is a weak maximum in the superconducting state observable in the raw data and the difference spectra in the temperature range 11-20 K.

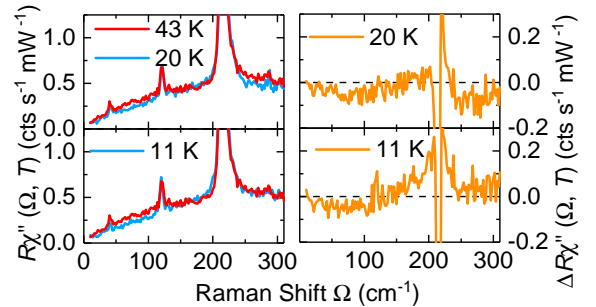


Figure A6. B_{2g} response of $\text{CaKFe}_4\text{As}_4$ for 43 K and temperatures below T_c as indicated. The raw response is shown on the left, the difference spectra are on the right.

- * Present address: Karlsruher Institut für Technologie, Institut für Festkörperphysik, 76021 Karlsruhe, Germany
- ¹ Akira Iyo, Kenji Kawashima, Tatsuya Kinjo, Taichiro Nishio, Shigeyuki Ishida, Hiroshi Fujihisa, Yoshito Gotoh, Kunihiro Kihou, Hiroshi Eisaki, and Yoshiyuki Yoshida, “New-Structure-Type Fe-Based Superconductors: $\text{CaAFe}_4\text{As}_4$ ($A = \text{K, Rb, Cs}$) and $\text{SrAFe}_4\text{As}_4$ ($A = \text{Rb, Cs}$),” *J. Am. Chem. Soc.* **138**, 3410–3415 (2016).
 - ² W. R. Meier, T. Kong, U. S. Kaluarachchi, V. Taufour, N. H. Jo, G. Drachuck, A. E. Böhmer, S. M. Saunders, A. Sapkota, A. Kreyssig, M. A. Tanatar, R. Prozorov, A. I. Goldman, Fedor F. Balakirev, Alex Gurevich, S. L. Bud’ko, and P. C. Canfield, “Anisotropic thermodynamic and transport properties of single-crystalline $\text{CaKFe}_4\text{As}_4$,” *Phys. Rev. B* **94**, 064501 (2016).
 - ³ Daixiang Mou, Tai Kong, William R. Meier, Felix Lochner, Lin-Lin Wang, Qisheng Lin, Yun Wu, S. L. Bud’ko, Ilya Eremin, D. D. Johnson, P. C. Canfield, and Adam Kaminski, “Enhancement of the Superconducting Gap by Nesting in $\text{CaKFe}_4\text{As}_4$: A New High Temperature Superconductor,” *Phys. Rev. Lett.* **117**, 277001 (2016).
 - ⁴ P. K. Biswas, A. Iyo, Y. Yoshida, H. Eisaki, K. Kawashima, and A. D. Hillier, “Signature of multigap nodeless superconductivity in $\text{CaKFe}_4\text{As}_4$,” *Phys. Rev. B* **95**, 140505 (2017).
 - ⁵ Run Yang, Yaomin Dai, Bing Xu, Wei Zhang, Ziyang Qiu, Qiangtao Sui, Christopher C. Homes, and Xiang-gang Qiu, “Anomalous phonon behavior in superconducting $\text{CaKFe}_4\text{As}_4$: An optical study,” *Phys. Rev. B* **95**, 064506 (2017).
 - ⁶ I. I. Mazin, D. J. Singh, M. D. Johannes, and M. H. Du, “Unconventional Superconductivity with a Sign Reversal in the Order Parameter of $\text{LaFeAsO}_{1-x}\text{F}_x$,” *Phys. Rev. Lett.* **101**, 057003 (2008).
 - ⁷ Peter J. Hirschfeld, “Using gap symmetry and structure to reveal the pairing mechanism in fe-based superconductors,” *C. R. Physique* **17**, 197 – 231 (2016), iron-based superconductors / Supraconducteurs base de fer.
 - ⁸ F. Kretzschmar, B. Muschler, T. Böhm, A. Baum, R. Hackl, Hai-Hu Wen, V. Tsurkan, J. Deisenhofer, and A. Loidl, “Raman-Scattering Detection of Nearly Degenerate s -Wave and d -Wave Pairing Channels in Iron-Based $\text{Ba}_{0.6}\text{K}_{0.4}\text{Fe}_2\text{As}_2$ and $\text{Rb}_{0.8}\text{Fe}_{1.6}\text{As}_2$ Superconductors,” *Phys. Rev. Lett.* **110**, 187002 (2013).
 - ⁹ T. Böhm, A. F. Kemper, B. Moritz, F. Kretzschmar, B. Muschler, H.-M. Eiter, R. Hackl, T. P. Devereaux, D. J. Scalapino, and Hai-Hu Wen, “Balancing act: Evidence for a strong subdominant d -wave pairing channel in $\text{Ba}_{0.6}\text{K}_{0.4}\text{Fe}_2\text{As}_2$,” *Phys. Rev. X* **4**, 041046 (2014).
 - ¹⁰ T. Böhm, F. Kretzschmar, A. Baum, M. Rehm, D. Jost, R. Hosseinian Ahangharnejhad, R. Thomale, C. Platt, T. A. Maier, W. Hanke, B. Moritz, T. P. Devereaux, D. J. Scalapino, S. Maiti, P. J. Hirschfeld, P. Adelman, T. Wolf, H.-H. Wen, and R. Hackl, “Microscopic pairing fingerprint of the iron-based superconductor $\text{Ba}_{1-x}\text{K}_x\text{Fe}_2\text{As}_2$,” ArXiv e-prints (2017), [arXiv:1703.07749](https://arxiv.org/abs/1703.07749) [cond-mat.supr-con].
 - ¹¹ A. Bardasis and J. R. Schrieffer, “Excitons and Plasmons in Superconductors,” *Phys. Rev.* **121**, 1050–1062 (1961).
 - ¹² H. Monien and A. Zawadowski, “Theory of Raman scattering with final-state interaction in high- T_c BCS superconductors: Collective modes,” *Phys. Rev. B* **41**, 8798–8810 (1990).
 - ¹³ D. J. Scalapino and T. P. Devereaux, “Collective d -wave exciton modes in the calculated Raman spectrum of Fe-based superconductors,” *Phys. Rev. B* **80**, 140512 (2009).
 - ¹⁴ W. R. Meier, T. Kong, S. L. Bud’ko, and P. C. Canfield, “Optimization of the crystal growth of the superconductor $\text{CaKFe}_4\text{As}_4$ from solution in the FeAs – CaFe_2As_2 – KFe_2As_2 system,” *Phys. Rev. Materials* **1**, 013401 (2017).
 - ¹⁵ Marianne Rotter, Marcus Tegel, and Dirk Johrendt, “Superconductivity at 38 K in the Iron Arsenide $(\text{Ba}_{1-x}\text{K}_x)\text{Fe}_2\text{As}_2$,” *Phys. Rev. Lett.* **101**, 107006 (2008).
 - ¹⁶ J.-R. Scholz, *Raman Scattering Study of the Superconducting Pairing in $\text{CaKFe}_4\text{As}_4$* , Master’s thesis, Technische Universität München (2017).
 - ¹⁷ W.-L. Zhang, W. R. Meier, T. Kong, P. C. Canfield, and G. Blumberg, “High T_c superconductivity in $\text{CaKFe}_4\text{As}_4$ in absence of nematic fluctuations,” ArXiv e-prints (2018), [arXiv:1804.06963](https://arxiv.org/abs/1804.06963) [cond-mat.supr-con].
 - ¹⁸ T. Cea and L. Benfatto, “Signature of the Leggett mode in the A_{1g} Raman response: From MgB_2 to iron-based superconductors,” *Phys. Rev. B* **94**, 064512 (2016).
 - ¹⁹ Thomas P. Devereaux and Rudi Hackl, “Inelastic light scattering from correlated electrons,” *Rev. Mod. Phys.* **79**, 175 (2007).
 - ²⁰ T. P. Devereaux, D. Einzel, B. Stadlober, R. Hackl, D. H. Leach, and J. J. Neumeier, “Electronic Raman scattering in high- T_c superconductors: A probe of $d_{x^2-y^2}$ pairing,” *Phys. Rev. Lett.* **72**, 396 (1994).
 - ²¹ I. I. Mazin, T. P. Devereaux, J. G. Analytis, Jiun-Haw Chu, I. R. Fisher, B. Muschler, and R. Hackl, “Pinpointing gap minima in $\text{Ba}(\text{Fe}_{0.94}\text{Co}_{0.06})_2\text{As}_2$ via band-structure calculations and electronic Raman scattering,” *Phys. Rev. B* **82**, 180502 (2010).
 - ²² M. P. Raphael, M. E. Reeves, and E. F. Skelton, “Nonlinear response of type II superconductors: A new method of measuring the pressure dependence of the transition temperature $T_c(P)$,” *Rev. Sci. Instrum.* **69**, 1451–1455 (1998).
 - ²³ S. Shatz, A. Shaulov, and Y. Yeshurun, “Universal behavior of harmonic susceptibilities in type-II superconductors,” *Phys. Rev. B* **48**, 13871 (1993).